

PLATE: Plasticity-Tunable Efficient Adapters for Geometry-Aware Continual Learning

Romain Cosentino

Abstract

We develop a continual learning method for pretrained models that *requires no access to old-task data*, addressing a practical barrier in foundation model adaptation where pretraining distributions are often unavailable. Our key observation is that pretrained networks exhibit substantial *geometric redundancy*, and that this redundancy can be exploited in two complementary ways. First, redundant neurons provide a proxy for dominant pretraining-era feature directions, enabling the construction of approximately protected update subspaces directly from pretrained weights. Second, redundancy offers a natural bias for *where* to place plasticity: by restricting updates to a subset of redundant neurons and constraining the remaining degrees of freedom, we obtain update families with reduced functional drift on the old-data distribution and improved worst-case retention guarantees. These insights lead to PLATE (**P**lasticity-**T**unable **E**fficient **A**dapters), a continual learning method requiring no past-task data that provides explicit control over the plasticity-retention trade-off. PLATE parameterizes each layer with a structured low-rank update $\Delta W = BAQ^\top$, where B and Q are computed once from pretrained weights and kept frozen, and only A is trained on the new task. The code is available at <https://github.com/SalesforceAIResearch/PLATE>.

1 Introduction

Deep neural networks trained sequentially on multiple tasks tend to forget what they have learned before: performance on old tasks degrades as the model is updated on new data [22, 30, 6, 8, 27]. In modern practice, a large backbone is first pretrained on a massive, opaque distribution, and is then adapted to downstream tasks via instruction tuning, domain adaptation, or reinforcement learning [25]. Fully fine-tuning all parameters on each new task is often too expensive and can severely erode core capabilities such as factual knowledge, reasoning, or instruction following.

Parameter-efficient fine-tuning (PEFT) has become the de facto solution to the cost side of this problem: instead of updating all parameters, one modifies only a small subset or a low-dimensional subspace of them using so called adapters [14, 20, 18, 15, 12]. These methods achieve strong performance on new tasks while training and storing only a small fraction of the backbone weights. However, PEFT alone does not eliminate catastrophic forgetting nor ensure the preservation of prior capabilities: even when only adapter parameters are trained, fine-tuning still erodes pretraining-era behavior and generalization [28, 41, 16]. Recent work has therefore begun to study continual learning specifically under PEFT. For instance, by using small auxiliary “context” sets to shape knowledge-preserving adapter subspaces [36] or forcing orthogonality between successive tasks [35]. In contrast, our approach targets the fully data-free setting with respect to the old task distribution: both the protected input subspace and the subset of trainable redundant neurons are inferred

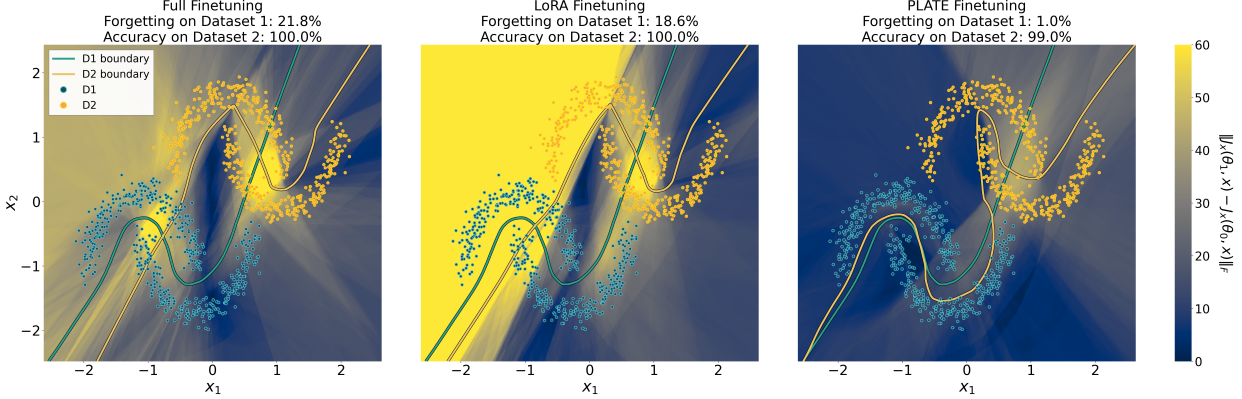


Figure 1: **Local-geometry view of forgetting on a continual learning 2-dimensional binary classification problem:** Blue points denote the old-task dataset P_0 and yellow points the new-task dataset P_1 ; decision boundaries are shown when trained on P_0 (blue curve) and after training on P_1 (yellow curve). The background heatmap visualizes how the training on P_1 change the model’s local input-output linearization, $\Delta(x) := \|J_x(\theta_1, x) - J_x(\theta_0, x)\|_F$. *Retention is compromised when the heatmap turns yellow around the blue points* (large drift on $\text{supp}(P_0)$), while *effective learning requires yellow regions around the yellow points* (large drift concentrated near $\text{supp}(P_1)$). *This motivates our goal: parameter-efficient continual updates that localize drift away from the (often unavailable) old distribution while remaining expressive on the new task.* (Left) Full fine-tuning induces large changes throughout, including on $\text{supp}(P_0)$, and the old boundary drifts. (Middle) LoRA restricts the parameter update but still produces substantial change on $\text{supp}(P_0)$. (Right) PLATE updates keep $\Delta(x)$ small on $\text{supp}(P_0)$ while permitting large changes near P_1 , concentrating plasticity where it is needed and preserving old behavior (see Figure 3 for PLATE hyperparameters sweep).

directly from frozen pretrained weights. To the best of our knowledge, PLATE is among the first continual-learning methods to derive *both* ingredients in a fully weight-only manner.

A natural way to mitigate forgetting is to constrain new-task updates so that they are “invisible” to the old task. Existing continual-learning methods implement this idea in different ways. Regularization-based approaches such as Elastic Weight Consolidation [17], Synaptic Intelligence [40], and Memory Aware Synapses [1] penalize movement along directions that were important for previous tasks. Replay and constrained-gradient methods [21, 3], use stored examples from old tasks to project gradients and reduce interference. Explicit orthogonality-based approaches such as Orthogonal Weight Modification and Orthogonal Gradient Descent [39, 4] estimate the feature subspace used by old tasks and project new gradients into its orthogonal complement. Architectural methods like Progressive Networks [31] and Dynamically Expandable Networks [37] go further by freezing old parameters and routing new tasks through newly added capacity. Mixture-of-Experts architectures have also been explored for continual learning by routing different tasks/inputs to specialized experts, reducing interference across tasks [19].

These strategies reduce forgetting to some extent, but they face serious limitations in the regime that motivates contemporary training approaches. First, most methods assume continued access to old-task data (or at least stored examples/gradients/features). In large-scale models,

this assumption is often violated: pretraining data are often proprietary, massive, and unavailable. Second, many approaches operate at the level of global gradients over the full model and are not computationally efficient at Large Language Model (LLM) scale. Third, even when old data are available, orthogonality constraints are inherently approximate: whether one estimates protected subspaces from stored data or from curvature surrogates such as Fisher information, feature statistics are noisy, nullspaces are only identified up to finite-sample and numerical error, and projections can only be enforced approximately. Finally, they are usually not applicable to the LLM scale because of their inherent computational burden.

In this work we ask: *Can we design a continual learning method that reduces forgetting without access to prior-task data, while remaining practical at scale?*

Our approach is motivated by two observations. First, orthogonality-based constraints alone do not eliminate forgetting: if the allowed update family is only approximately orthogonal to old-task features, then there exist directions within it that still induce a non-trivial increase in the old-task loss. Second, pretrained models exhibit substantial redundancy: many neurons implement highly similar features, often visible as strong colinearity among weight vectors, a phenomenon induced by overparameterization, dropout, and the implicit bias of training dynamics [34, 2, 38].

This suggests two complementary opportunities for continual learning without past-task data: (i) redundancy can serve as a *weight-only proxy* for dominant old-task feature directions, enabling approximate protected subspaces computed directly from frozen weights, (ii) redundancy can guide *where to place plasticity*: concentrating updates on redundant neurons biases adaptation toward directions that are empirically less function-changing on the original distribution.

These insights motivate PLATE (**P**lasticity-**T**unable **E**fficient **A**dapters), a PEFT method that implements exactly this recipe. At each layer, before training, PLATE (i) identifies a set of trainable redundant neurons from frozen weights, (ii) builds a low-energy input subspace from the complement (frozen) neurons, both contributing to the protection of the pre-training distribution of the model. We parameterize the model updates as a low-rank adapter: concretely, each adapted layer uses updates of the form $B^{(\ell)} A^{(\ell)} Q^{(\ell)\top}$, where $B^{(\ell)}$ (frozen) selects redundant output neurons, $Q^{(\ell)}$ (frozen) spans a weight-based approximate pre-training distribution nullspace, and $A^{(\ell)}$ are trainable parameters. This yields a parameter efficient geometry-aware adapter that requires no access to pretraining data, exposes an explicit plasticity trade-off via the estimated (resp. selected) input (resp. output) dimensions of the A matrix, and inherits the computational benefits of PEFT methods.

The paper is organized as follows: (i) We show that any approximately protected update family admits a nonzero worst-case forgetting floor and provide a weight-only construction of approximate protected directions from pretrained redundancy (Sections 2). (ii) We relate worst-case forgetting over an update family to old-task restricted curvature, and upper bound this curvature by first-order functional drift (Sections 3). (iii) We propose PLATE, a data-free continual PEFT adapter $\Delta W = BAQ^\top$ that concentrates plasticity on redundant channels and restricts updates to a low-energy input subspace computed once from frozen weights (Section 4). (iv) Across controlled continual-learning benchmarks and LLM specialization, PLATE improves retention over LoRA [15] at similar trainable budgets while preserving new-task performance (Section 5).

2 Data-Free Constraints for Continual Learning

This section develops three ingredients for data-free continual learning: (i) an exact invariance condition that yields zero forgetting but requires access to P_0 , (ii) a lower bound showing why approximate orthogonality admits a worst-case forgetting floor, and (iii) a weight-only route to approximate protected subspaces via redundancy.

In this paper, we generally consider a two-task continual-learning setting. An old task is represented by a distribution P_0 over (x, y) and a new task by P_1 . A network f_θ is trained on P_0 to obtain parameters θ_0 , and then adapted on P_1 to obtain $\theta_1 = \theta_0 + \Delta\theta$. We define $L_0(\theta) := \mathbb{E}_{(x,y) \sim P_0} [\ell(f_\theta(x), y)]$ and $L_1(\theta) := \mathbb{E}_{(x,y) \sim P_1} [\ell(f_\theta(x), y)]$ as the old- and new-task losses, respectively. The forgetting on P_0 is $\mathcal{F}_0(\theta_0, \theta_1) := L_0(\theta_1) - L_0(\theta_0)$.

2.1 Layerwise exact invariance orthogonality

Let $h_\theta^{(\ell)}(x)$ denote the post-activation of layer ℓ and $z_\theta^{(\ell)}(x)$ its pre-activation. Ignoring biases for clarity

$$z_\theta^{(\ell)}(x) = W^{(\ell)} h_\theta^{(\ell-1)}(x), \quad h_\theta^{(\ell)}(x) = \sigma(z_\theta^{(\ell)}(x)).$$

For an update $\Delta\theta = \{\Delta W^{(\ell)}\}_\ell$, we define a point-wise orthogonality condition on P_0 .

Definition 1 (Layerwise, per-sample orthogonality on P_0). We say that $\Delta\theta$ is *per-layer orthogonal on P_0* if for every layer ℓ and every $x \in \text{supp}(P_0)$

$$\Delta W^{(\ell)} h_{\theta_0}^{(\ell-1)}(x) = 0. \quad (1)$$

Proposition 1 (Per-layer orthogonality yields no forgetting (Proof in Appendix A.1)). *If $\Delta\theta$ satisfies (1), then $\mathcal{F}_0(\theta_0, \theta_0 + \Delta\theta) = 0$.*

Proposition 1 is an exact invariance statement. Its limitation is practical: enforcing (1) requires access to old-task features $h_{\theta_0}^{(\ell-1)}(x)$ over $\text{supp}(P_0)$ and building an orthogonal complement (or projector) to their span, which is infeasible when the old distribution is unavailable and costly even when a replay buffer exists.

2.2 Approximate orthogonality implies a forgetting floor

In practice, orthogonality constraints are approximate. We quantify approximation using a first-order linearization and a distributional drift measure.

For small $\Delta\theta$, we use the following first-order linearization

$$f_{\theta_0 + \Delta\theta}(x) \approx f_{\theta_0}(x) + J_{\theta_0}(x)\Delta\theta,$$

where $J_{\theta_0}(x) := \nabla_\theta f_\theta(x)|_{\theta=\theta_0}$ is the Jacobian of the model output with respect to the parameters, evaluated at θ_0 . Thus $J_{\theta_0}(x)\Delta\theta$ gives the first-order change in the output at input x induced by the parameter perturbation $\Delta\theta$.

To measure this drift under $x \sim P_0$, we define $\|J_{\theta_0}\Delta\theta\|_{L_2(P_0)} := (\mathbb{E}_{x \sim P_0} [\|J_{\theta_0}(x)\Delta\theta\|_2^2])^{1/2}$. Now, If updates are restricted to a linear subspace $S \subset \mathbb{R}^{\dim(\theta)}$, we define the worst-case unit-norm drift radius as

$$\varepsilon(S) := \sup_{\|\Delta\theta\|_2=1, \Delta\theta \in S} \|J_{\theta_0}\Delta\theta\|_{L_2(P_0)}. \quad (2)$$

In particular, $\varepsilon(S) = 0$ means that $J_{\theta_0}(x)\Delta\theta = 0$ for all $x \in \text{supp}(P_0)$ and all $\Delta\theta \in S$, i.e., updates in S induce no *first-order* output change on old inputs. This is a linearized analogue of the exact invariance in Proposition 1. Note that $\varepsilon(S)$ provides a quantitative measure of how “orthogonal” the update subspace S is to the old-task features: it captures the worst-case first-order output drift on P_0 induced by a unit-norm update in S . Figure 1 provides an input-space visualization of this notion of drift: the heatmap tracks changes in the local input–output linearization around old and new data samples.

We now denote by $g_0 := \nabla_{\theta}L_0(\theta_0)$ and $H_0 := \nabla_{\theta}^2L_0(\theta_0)$ the loss gradient and Hessian at θ_0 . Note that, for a model that has been well-optimized on P_0 , we typically have $g_0 \approx 0$, so small-step changes in L_0 are dominated by the quadratic term governed by H_0 .

The following theorem shows that as soon as $\varepsilon(S) > 0$, e.g., as soon as orthogonality is only approximate, there always exists a direction inside S that incurs a non-trivial amount of forgetting.

Theorem 1 (Lower bound on worst-case forgetting under approximate orthogonality (Proof in Appendix A.2)). *Assume a curvature link between H_0 and J_{θ_0} (Assumption 1 in Appendix A.2), then, there exist constants $c > 0$ and $\rho > 0$ such that $\exists \Delta\theta \in S$ with $\|\Delta\theta\|_2 = \rho$ for which*

$$\mathcal{F}_0(\theta_0, \theta_0 + \Delta\theta) \geq c\rho^2\varepsilon(S)^2 + O(\rho^3)$$

where $c > 0$ depends only on local properties of L_0 around θ_0 , in particular the curvature-link in Assumption 1.

In other words, approximate protection leaves an unavoidable worst-case forgetting floor. As soon as $\varepsilon(S) > 0$, meaning the update family S permits some nonzero first-order output drift on old inputs, there exists a direction in S that increases the old-task loss by at least $\rho^2\varepsilon(S)^2$ for sufficiently small step size ρ .

2.3 Data-free protected subspaces from neuron redundancy

Orthogonality-based continual-learning methods estimate protected subspaces from old-task data (e.g., gradients or feature covariances) and constrain updates accordingly. In large pretrained models, the pretraining distribution P_0 is typically unavailable (and replay is often infeasible), motivating a *weight-only* proxy for old-feature directions.

Pretrained networks are highly redundant and compressible [10, 11, 13, 5], implying that many neurons capture repeated directions. An explanation for why such repeated directions are tied to the data distribution is provided by deep neural collapse analyses. In particular, [7] derive an explicit deep neural collapse structured solution form in a deep linear unconstrained-features model. A key consequence is that, at each layer, weight vectors are confined to a low-dimensional data-dependent subspace.

Proposition 2 (Layerwise weights lie in a data-dependent prototype subspace [7] (Proof in Appendix A.3)). *For each layer ℓ there exist prototype directions $\{\mu_c^{(\ell)}\}_{c=1}^K$ (per layer class-mean feature directions) such that every row $w_j^{(\ell)}$ of $W^{(\ell)}$ satisfies $w_j^{(\ell)} \in \text{span}\{\mu_1^{(\ell)}, \dots, \mu_K^{(\ell)}\}$.*

Proposition 2 shows that at each layer, the trained weights concentrate in a low-dimensional subspace determined by the data. In a wide layer, this naturally leads to a large number of colinear weights within that subspace.

Motivated by Proposition 2, we treat densely repeated (high-cosine-similarity) neuron directions as a weight-only proxy for dominant pretraining-era feature directions. Concretely, by grouping colinear neurons and taking the orthogonal complement of their span, we obtain an update subspace intended to suppress interaction with the most salient old-task features as an approximation to Proposition 1. This yields a data-free route to an *approximately* protected update family with small (but generally nonzero) drift radius $\varepsilon(S)$, and therefore still inherits the nonzero worst-case floor from Theorem 1. In the next section we complement approximate input-side protection with an explicit drift control lens, and later instantiate it via redundant-neuron plasticity.

3 Low-Curvature Update Families

Theorem 1 shows that approximate orthogonality alone leaves a non-zero worst-case forgetting floor whenever $\varepsilon(S) > 0$. We now introduce a complementary geometric point of view: the *restricted curvature* of the old-task loss over an update family S . This allows us to derive upper bounds on worst case forgetting and understand how one can build an update subspace S that will mitigate forgetting.

3.1 A local quadratic view of worst-case forgetting

We now consider the old-task loss L_0 around θ_0

$$L_0(\theta_0 + \Delta\theta) \approx L_0(\theta_0) + g_0^\top \Delta\theta + \frac{1}{2} \Delta\theta^\top H_0 \Delta\theta,$$

where $g_0 = \nabla_\theta L_0(\theta_0)$ and $H_0 = \nabla_\theta^2 L_0(\theta_0)$. For a well-trained model, $g_0 \approx 0$ and the quadratic term dominates small-update forgetting, consistent with loss-landscape analyses that connect retention to the geometry of task optima and the widening effect of training regimes [23]. For a linear update family subspace S , define its *restricted curvature*

$$\lambda(S) := \sup_{\substack{\Delta\theta \in S, \\ \|\Delta\theta\|_2=1}} \Delta\theta^\top H_0 \Delta\theta.$$

To capture worst-case behaviour, define the local worst-case forgetting over the update family subspace S

$$\mathcal{F}_{\max}(S, \rho) := \sup_{\substack{\Delta\theta \in S \\ \|\Delta\theta\|_2 \leq \rho}} \mathcal{F}_0(\theta_0, \theta_0 + \Delta\theta).$$

Proposition 3 (Upper bound via restricted curvature (Proof in Appendix A.4)). $\exists \rho > 0$ such that for any linear subspace S

$$\mathcal{F}_{\max}(S, \rho) \leq \frac{\lambda(S)}{2} \rho^2 + O(\rho^3).$$

In particular, for unconstrained full fine-tuning, $\mathcal{F}_{\max}(\mathbb{R}^{\dim(\theta)}, \rho) \leq \frac{\lambda_{\max}}{2} \rho^2 + O(\rho^3)$, where λ_{\max} is the largest eigenvalue of H_0 .

Proposition 3 provides a design principle: to reduce worst-case forgetting, choose S so that it *removes* high-curvature directions of the old loss. However, $\lambda(S)$ depends on the restriction of the old-task Hessian H_0 to S , which is generally intractable to compute and hard to approximate reliably without old-task data. We now show that under some assumptions, $\lambda(S)$ can be controlled by the *first-order* functional drift radius $\varepsilon(S)$ from Section 2.2.

3.2 From curvature to functional drift

We now connect the local worst-case forgetting control knob from Section 3.1, the *restricted curvature* $\lambda(S)$, to the *functional drift* that is directly targeted by orthogonality-style constraints. Recall the drift radius $\varepsilon(S)$ from Eq. 2 measures the worst-case *first-order* change in the model output on old-task inputs induced by a unit-norm update restricted to S .

For well-trained pretrained models, the old-task loss is typically close to stationary on the old distribution, so higher-order effects are weak and the curvature along an update direction is well captured by how much that update changes the model’s outputs on old inputs.

Proposition 4 (Restricted curvature is bounded by functional drift (Proof in Appendix A.5)). *Assume there exists $\beta > 0$ such that $\nabla_f^2 \ell(f_{\theta_0}(x), y) \preceq \beta I$, then for any linear subspace S*

$$\lambda(S) \leq \beta \varepsilon(S)^2.$$

Proposition 4 allows us to connect a second-order quantity $\lambda(S)$ on the loss into a first-order one $\varepsilon(S)$ on the network mapping. Specifically, it describes that if an update family produces small first-order output drift on P_0 , then it cannot expose large old-task curvature.

Combining Proposition 3 (worst-case forgetting is controlled by $\lambda(S)$) with Proposition 4 (restricted curvature is controlled by $\varepsilon(S)$) yields the following upper bound on worst case forgetting.

Theorem 2 (Worst-case forgetting is controlled by functional drift (Proof in Appendix A.6)). *There exist $\rho > 0$ such that for any linear subspace S*

$$\mathcal{F}_{\max}(S, \rho) \leq \frac{\beta}{2} \varepsilon(S)^2 \rho^2 + O(\rho^3).$$

Theorem 2 shows that *to reduce local worst-case forgetting, it suffices to construct update families with small drift radius $\varepsilon(S)$ on P_0* . The remaining question is: how can we design such low-drift update families without access to P_0 ?

3.3 Designing low-drift update families without access to old-task data

The key ingredient to design such a low-drift update family without having to access the old-task data is redundancy in pretrained layers: deep neural networks are highly compressible [11, 10, 13, 5, 24], and this redundancy is often expressed as repeated/colinear weight directions and near-duplicate features [38, 2]. We leverage this on the input side (approximate protection) and the output side (restricting plasticity to redundant channels):

1. **Input-side protection (weight-only approximate data-orthogonality).** Motivated by the weight-only construction in Section 2.3 and the drift-based design target in Section 3.3, we build an *approximately protected* input subspace using redundancy: we group highly colinear neurons (a proxy for dominant pretraining-era feature directions) and use its orthogonal subspace to suppress interaction with those directions. This mirrors orthogonality-style continual-learning constraints [39, 4, 32], but in a fully data-free, weight-only manner, leveraging redundancy and compressibility in trained networks.
2. **Output-side safety (redundant-channel restriction).** Motivated by the fact that approximate orthogonality alone admits a worst-case forgetting floor (Section 2.2) and by the

drift/curvature control perspective (Sections 3.1-3.2), we further concentrate plasticity on a subset of *highly redundant* neurons. In fact, redundant neurons exhibit colinear hyperplanes and does not induce new partitions in the network input space. This biases updates toward degrees of freedom that are empirically shown to reduce the drift of the network mapping on the pre-trained data, consistent with geometric views introduced in [2, 38] and broader evidence of redundancy in overparameterized trained networks [10, 11, 5, 13].

Together, these two restrictions define a structured, low-dimensional update family that is explicitly designed to reduce old-task drift $\varepsilon(S)$ using only pretrained weights.

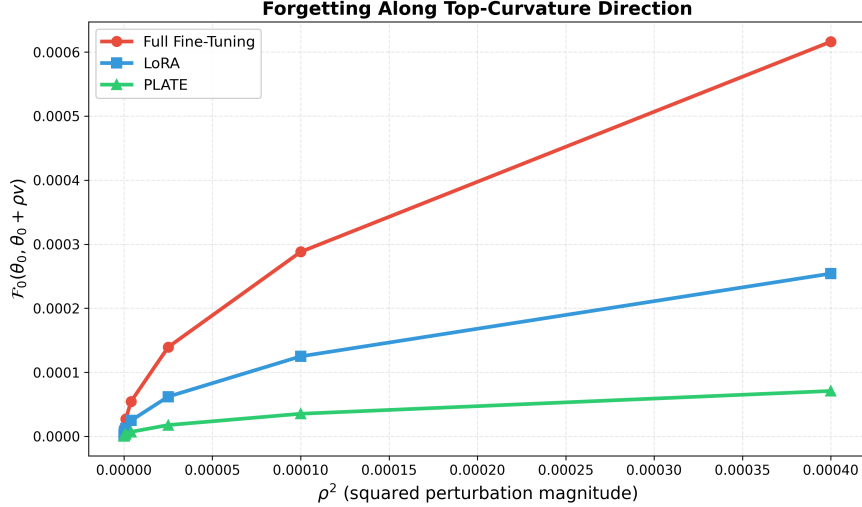


Figure 2: **Restricted-curvature forgetting:** We train an MLP on MNIST digits 0-4 to obtain parameters θ_0 . For each method, we perturb the trained model by $\theta_0 + \rho v$ and measure the resulting forgetting $\mathcal{F}0(\theta_0, \theta_0 + \rho v) = L_0(\theta_0 + \rho v) - L_0(\theta_0)$ where v is the unit vector in each subspace that maximizes $v^T H_0 v$, i.e., *highest-curvature direction*. PLATE exhibits the smallest slope, indicating substantially reduced restricted curvature and correspondingly smaller worst-case forgetting.

Figure 2 empirically supports the restricted-curvature perspective: even within a parameter-efficient family, the old-task loss can increase rapidly if the family still contains high-curvature directions. In this MNIST experiment, LoRA’s low-rank tangent subspace still exposes directions with relatively large restricted curvature, whereas PLATE’s structured family exhibits a smaller slope. This is consistent with PLATE’s two weight-only restrictions: (i) restricting plasticity to a subset of redundant output channels and (ii) constraining updates to a low-energy input subspace inferred from frozen weights, both designed to reduce drift.

4 PLATE: Plasticity-Tunable Efficient Adapters

We now instantiate these principles in a parameter-efficient adapter-based method that is fully data-free with respect to the old distribution P_0 . The resulting method, PLATE (**P**lasticity-**T**unable **E**fficient **A**dapters), constructs for each adapted linear map a structured update family that is designed to reduce $\varepsilon(S)$ using only frozen pretrained weights: (i) it concentrates plasticity on a

Algorithm 1 PLATE

Require: Pretrained model parameters θ_0 , target linear layers \mathcal{L} , number of selected output neurons r , energy threshold for input subspace $\tau \in (0, 1)$, scaling ρ

- 1: **for** each layer $\ell \in \mathcal{L}$ with weight $W^{(\ell)} \in \mathbb{R}^{d_{\text{out}} \times d_{\text{in}}}$ **do**
- 2: **Redundant-output selection:** choose indices $\mathcal{I}^{(\ell)}$ of cardinal r using neuron similarity measure (Section 4.2)
- 3: Form $B^{(\ell)} = [e_i]_{i \in \mathcal{I}^{(\ell)}} \in \mathbb{R}^{d_{\text{out}} \times r}$, where e_i denotes the i -th standard basis vector in $\mathbb{R}^{d_{\text{out}}}$
- 4: Let $W_{\text{frozen}}^{(\ell)}$ be the submatrix of rows *not* in $\mathcal{I}^{(\ell)}$
- 5: **Low-energy input basis:** compute $Q^{(\ell)} \in \mathbb{R}^{d_{\text{in}} \times k}$ from $W_{\text{frozen}}^{(\ell)}$ (Section 4.3), where k is chosen so the *complementary* high-energy subspace captures a τ fraction of the estimated energy
- 6: Initialize trainable $A^{(\ell)} \in \mathbb{R}^{r \times k}$ (zero matrix)
- 7: Define the adapted layer by $W'^{(\ell)} = W^{(\ell)} + \rho B^{(\ell)} A^{(\ell)} Q^{(\ell)\top}$
- 8: **end for**
- 9: Train only $\{A^{(\ell)}\}_{\ell \in \mathcal{L}}$ on the new-task data (all $W^{(\ell)}, B^{(\ell)}, Q^{(\ell)}$ frozen)

subset of *redundant* output channels and (ii) it restricts updates to a *low-energy* input subspace inferred from the remaining frozen weights.

Specifically, for each layer ℓ , PLATE defines a linear update family

$$S_{\text{PLATE}}^{(\ell)} := \{ B^{(\ell)} A^{(\ell)} Q^{(\ell)\top} : A^{(\ell)} \in \mathbb{R}^{r \times k} \},$$

where $B^{(\ell)} \in \mathbb{R}^{d_{\text{out}} \times r}$ is an *index-selection matrix* (a column submatrix of the identity) that selects r trainable (redundant) output channels, $Q^{(\ell)} \in \mathbb{R}^{d_{\text{in}} \times k}$ spans a low-energy input subspace, and only $A^{(\ell)}$ is learned. Similar to LoRA and other PEFT methods, PLATE adds an adapter to the frozen modules that are selected for fine-tuning.

$$W' = W + \rho \Delta W, \quad \Delta W = BAQ^\top.$$

PLATE adapter adds a rank $\leq \min(r, k)$ matrix to the existing frozen weight with rk trainable parameters. The pseudo-code is described in Algorithm 1 and its computational complexity analysis of the algorithm is provided in Section 5.4 (Figure 9 for computational comparison with LoRA on DistilBERT fine-tuning).

4.1 Algorithm overview

PLATE consists of a one-time, weight-only preprocessing step per layer to compute (B, Q) , followed by standard adapter training on the new-task data with only A trainable. The key point is that both ingredients are computed *once per model and without access to P_0* . In Figure 10 we provide details regarding the complexity of PLATE initialization.

PLATE exposes two main hyperparameters that have provide an explicit trade-off between learning and forgetting: (i) r the number of adapted (redundant) output neurons, which controls the *plasticity budget*. Increasing r typically improves learnability on the new task but can increase old-task forgetting as it increase the number of learnable neurons and therefore affect $\varepsilon(S)$, (ii) τ an input energy threshold controlling the size of the orthogonal subspace, k . That is, τ controls how conservatively PLATE restricts updates to redundant degrees of freedom. Note that *larger* τ makes

the constraint more stringent and induces a *smaller* k , because k is chosen as the *smallest* dimension such that the complementary (high-energy) subspace captures a τ fraction of the spectrum/energy of W_{frozen} .

It is important to note that the additional flexibility PLATE offers in navigating the learning-forgetting trade-off comes at the cost of more involved engineering choices than simpler PEFT methods such as LoRA. Also, one should note that the number of learnable parameters for LoRA and PLATE scale differently from the rank r . In fact, LoRA learnable parameters per layer are *2rd* while for PLATE, there is no dependency on the number of hidden dimension, that is, the number of learnable parameters is rk . This is a crucial difference as in PLATE one can increase the rank while not drastically increasing the number of parameters as the hidden dimension d is usually large in LLMs.

4.2 Constructing the redundant-neuron selector B

The first mechanism to reduce drift is to restrict plasticity to *redundant* output channels (Section 3.3). Intuitively, if a layer’s output direction is implemented repeatedly by many other neurons, then modifying one instance tends to induce smaller functional change on the pretrained representation, and reduces drift on old inputs (Section 2.3).

As theoretically justified for pruning in [38], PLATE selects trainable output neurons using a simple redundancy heuristic: output rows that are highly colinear with many others are treated as redundant and are therefore candidates for plasticity (see also Section 3.3). Concretely, for each layer we score each output neuron w_i^\top of W by an estimate of its average cosine similarity to a set of *anchor* rows, and we pick the top- r rows using this score.

To scale to large d_{in} , we compute similarities in a random projection space. Let $R \in \mathbb{R}^{d_{\text{in}} \times d'}$ be a random Gaussian projection (with $d' \ll d_{\text{in}}$) and define

$$z_i = \frac{w_i^\top R}{\|w_i\|_2} \in \mathbb{R}^{d'}$$

We choose a set of anchor indices \mathcal{A} , and score each neuron by

$$s_i = \frac{1}{|\mathcal{A}|} \sum_{j \in \mathcal{A}} |\langle z_i, z_j \rangle|. \quad (3)$$

PLATE sets \mathcal{I} to the indices of the r largest scores $\{s_i\}$ and defines $B = [e_i]_{i \in \mathcal{I}}$.

Rows with high s_i lie in densely populated directions of row space (directions implemented repeatedly by many neurons). Concentrating plasticity on these rows is therefore a pretrained distribution data-free bias toward update directions that induce smaller functional drift on the pretrained behavior.

4.3 Constructing the weight-derived input basis Q

The second mechanism to reduce drift is to constrain the input side of the update to directions that are “low-energy” with respect to the frozen part of the layer as a proxy to “low-energy” P_0 data directions. The design choice is that Q is computed from the *complement* of the selected trainable rows.

Let \mathcal{I} be the selected indices and define the frozen-row submatrix

$$W_{\text{frozen}} \in \mathbb{R}^{(d_{\text{out}}-r) \times d_{\text{in}}} \text{ by removing rows indexed by } \mathcal{I},$$

and consider its Gram matrix $G_{\text{in}} := W_{\text{frozen}}^\top W_{\text{frozen}} \in \mathbb{R}^{d_{\text{in}} \times d_{\text{in}}}$. This low-energy (bottom-eigenspace) construction is the same weight-only protected input subspace described in Section 2.3: it corresponds to the (approximate) nullspace of W_{frozen} , i.e., directions orthogonal to the span of frozen neurons (our proxy for dominant pretraining-era feature directions).

Directions with small quadratic form under G_{in} correspond to inputs that weakly excite the frozen neurons. PLATE defines Q as an orthonormal basis spanning a *low-energy* subspace of G_{in} , i.e., Q approximates the bottom-eigenspace of G_{in} . Restricting updates to this subspace is intended to limit interaction with dominant pretrained features, and thus reduce first-order output drift on old inputs.

PLATE selects the basis dimension k using a threshold $\tau \in (0, 1)$: k is chosen so that the complementary (high-energy) subspace captures approximately a τ fraction of the estimated energy, and k is capped by k_{max} . This yields an explicit *plasticity knob*: larger τ (inducing smaller k) enforces stricter input constraints and typically improves retention.

When d_{in} is large, PLATE avoids forming G_{in} explicitly and instead uses a structured randomized Hadamard transform (SRHT) together with batched Hutchinson-style probes to estimate low-energy directions efficiently. Concretely, PLATE (i) applies an SRHT rotation, (ii) screens candidate coordinates using coarse then refined probes, and (iii) polishes within the candidate span by solving a small eigenproblem to recover a k -dimensional low-energy subspace.

Figure 3 shows a parameter sweep on a two-moons continual-learning setup. In this figure the Jacobian-drift heatmap $\Delta(x) = \|J_x(\theta_1, x) - J_x(\theta_0, x)\|_F$ provides a fine-grained view of *where* the model’s local geometry changes under adaptation: PLATE can concentrate change near the new-task support while keeping drift small near the old-task support.

5 Experiments

In this section, we provide the experimental results for PLATE. We evaluate PLATE in two complementary regimes:

1. **Out-of-distribution forgetting in LLMs:** we adapt pretrained LLMs on new reasoning / instruction-following dataset and probe both forgetting and learnability on *separate* benchmarks that were not used in training (Section 5.2). Training performed with open-instruct¹ and evaluation with OLMES [9].
2. **In-distribution forgetting in controlled benchmarks:** we build standard two-task continual-learning setups in vision, regression, and text where the evaluation distribution coincides with a known training distribution (Section 5.3). For this experiments we follow the conventional two-stage continual-learning protocol described in Appendix 2.

For the out-of-distribution LLM experiments, we compare LoRA and PLATE. Across all in-distribution experiments, we compare Full FT (all weights trainable), LoRA, and PLATE. We also want to remind that as aforementioned, although PLATE has a higher rank than LoRA does not

¹<https://github.com/allenai/open-instruct>

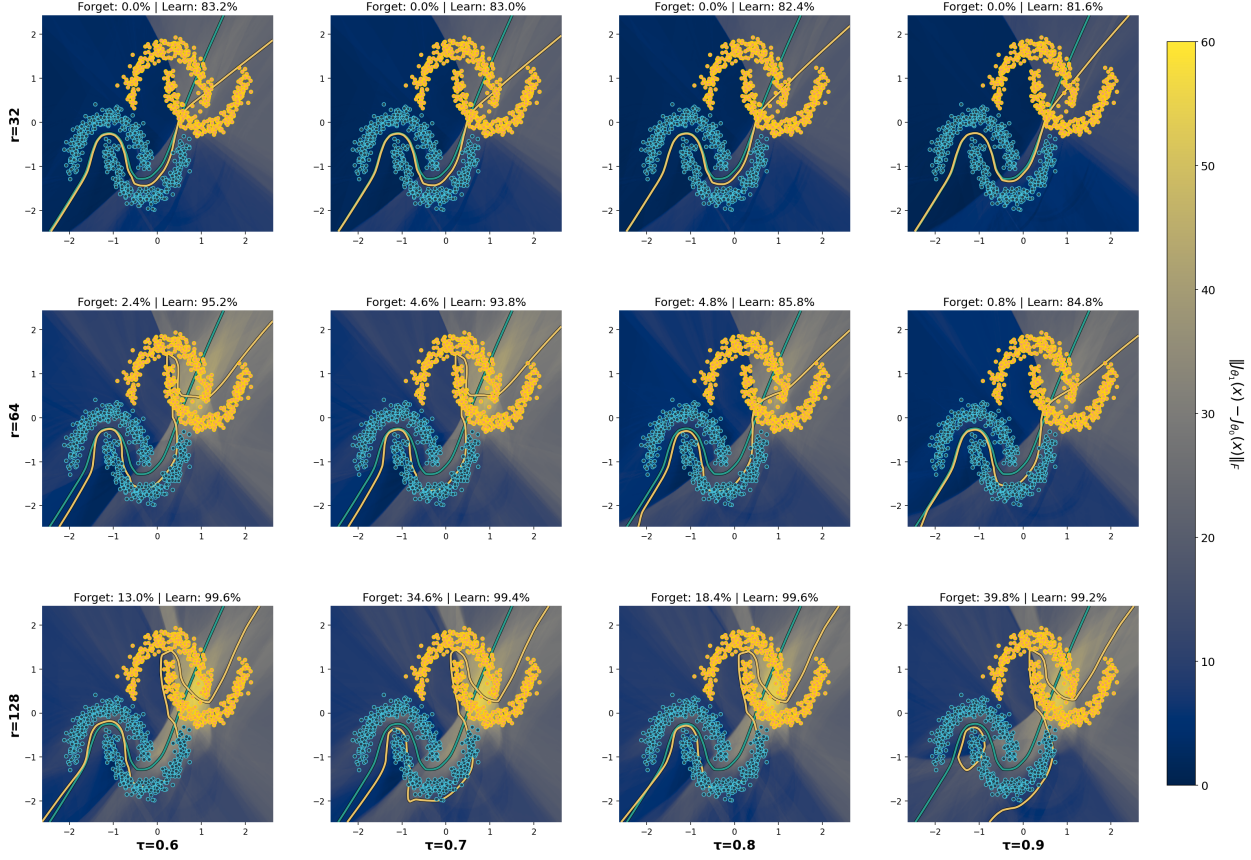


Figure 3: **PLATE exhibits a controllable forgetting-plasticity spectrum via (r, τ) :** We sweep PLATE’s hyperparameters on a two-moons continual-learning toy: the number of adapted (redundant) output neurons r (rows) and the input energy threshold τ (columns), where larger τ enforces a stricter input-side constraint (smaller k). Each panel overlays Dataset 1 (blue) and Dataset 2 (yellow), and visualizes how adaptation changes the model’s local input-output geometry using the Jacobian-drift heatmap $\Delta(x) = \|J_x(\theta_1, x) - J_x(\theta_0, x)\|_F$. We report *forgetting* on dataset 1 and *learning* accuracy on dataset 2. Increasing r expands the plasticity budget and improves dataset 2 performance but can increase dataset 1 drift/forgetting, while increasing τ tends to concentrate updates onto more redundant degrees of freedom and reduces drift/forgetting. Overall, PLATE provides an explicit mechanism to target a desired point on the retention-adaptation trade-off.

imply that PLATE has more learnable parameters. We also emphasize that forgetting is often easier to anticipate in traditional deep learning settings than in out-of-distribution LLM experiments. In practice, LLM fine-tuning corpora are highly heterogeneous and frequently overlap with many aspects of the model’s pretraining mixture (e.g., literature, math, reasoning, law, code), so it is rarely clear which capabilities are actually being reinforced versus overwritten. Moreover, the extreme scale at which LLMs operate makes their adaptation dynamics harder to predict: retention can vary substantially with the base model, the fine-tuning data, and the optimization setup, and small

changes in any of these can lead to qualitatively different forgetting behavior.

5.1 General protocol

All two-task experiments share the same structure, summarized in Algorithm 2. We either first train on task 1, checkpoint the resulting model, or used the pre-trained model, and then adapt independently to task 2 with each method/hyperparameter configuration. We either use a pre-trained LLM (for the OOD experiments) or we train a base model f_θ with task 1 head h_1 on \mathcal{D}_1 for E_1 epochs and record the baseline performance $\text{acc}_1^{\text{base}}$ on $\mathcal{D}_1^{\text{test}}$. Then, starting from the saved checkpoint, we apply either full fine-tuning, LoRA, or PLATE to the backbone f_θ . For the in-domain experiments, the task 1 head h_1 is frozen, while a new task 2 head h_2 is randomly initialized and trained on \mathcal{D}_2 for E_2 epochs. We then evaluate both task 2 performance (learnability) and task 1 retention (forgetting). We report in Table 1 and Table 2 the hyperparameters configurations and the hyperparameters we sweep for each experiments. Specifically, we cross-validate LoRA rank r (keeping α/r fixed) and PLATE’s neuron rank r , basis dimension threshold τ . Note that for all the experiments, we set the scaling of the adapter (α/r for LoRA and ρ for PLATE) to be set to 0.5 as to only capture the structural learning differences.

5.2 Out-of-distribution forgetting in LLM specialization

We first consider the LLM setting where the pretraining distribution P_0 is unknown and inaccessible, and we evaluate forgetting on *OOD* benchmarks to analyze how much fine-tuning affect the generalization capabilities of the model.

5.2.1 Qwen2.5-7B specialized to DeepSeek-R1 reasoning dataset

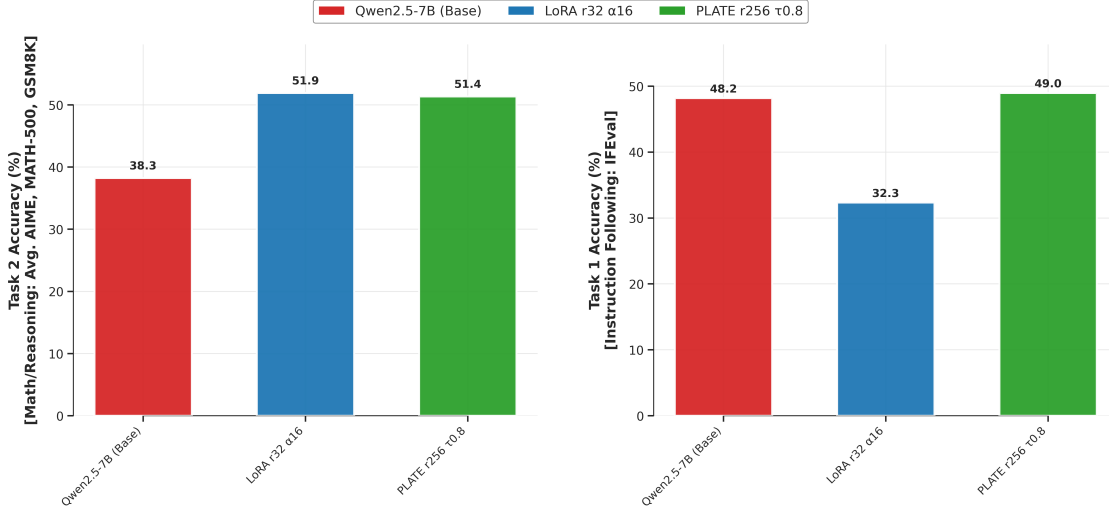


Figure 4: **Qwen2.5-7B on DeepSeek-R1 reasoning:** (Left) Learning capabilities on maths/reasoning dataset. (Right) Forgetting on instruction following dataset. PLATE (green) matches LoRA (blue) on math/reasoning benchmarks while preserving instruction-following (IFEval), whereas LoRA exhibits substantial OOD forgetting relative to the base model.

We start with Qwen2.5-7B [29] and fine-tune on it the AM-DeepSeek-R1 distilled reasoning corpus using the `open_instruct` package (1 epoch, learning rate 10^{-4} , AdamW). We compare: (1) base model, (2) LoRA (rank 32), and (3) PLATE (rank 256), adapters are attached to all modules. We evaluate (i) **OOD learning** on math/reasoning benchmarks (AIME, GSM8K, MATH-500) that are somewhat OOD with respect to DeepSeek-R1; and (ii) **OOD forgetting** on IFEval, which probes instruction-following capabilities acquired during pretraining. Figure 4 shows that PLATE matches LoRA’s $\approx +13$ point gain on math while essentially eliminating the ≈ 16 point drop that LoRA incurs on IFEval.

5.2.2 OLMo-2-7B Specialized to Tulu-3 dataset

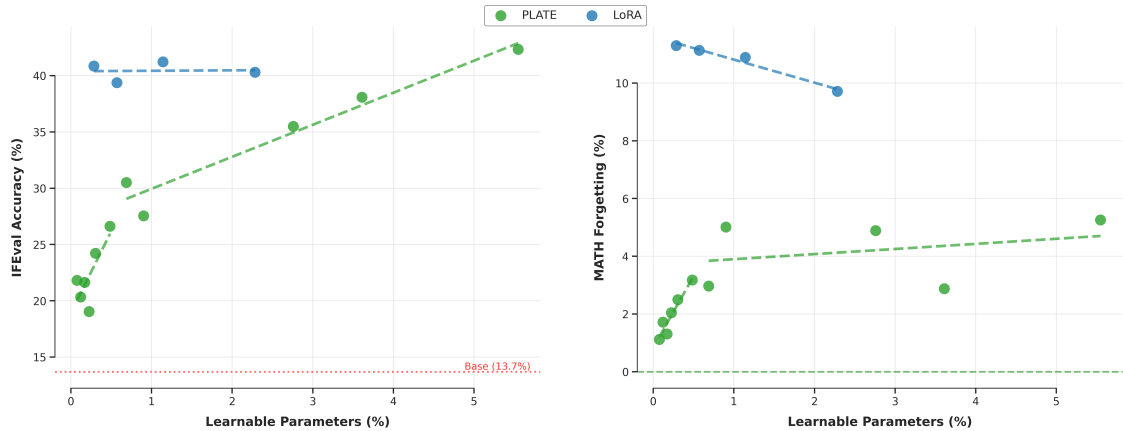


Figure 5: **OLMo-2-7B on Tulu-3:** (Left) IFEval accuracy vs. percentage of trainable parameters. The red dashed line is the base model capabilities on IFEval. (Right) MATH forgetting (drop from base) versus trainable parameters. PLATE (green) improves IFEval roughly linearly with parameter budget while keeping forgetting almost flat, whereas LoRA (blue) quickly saturates on IFEval and accumulates much larger MATH forgetting.

We then study how the percentage of learnable parameters affect both learning and forgetting capabilities. The base model is OLMo-2-7B [26], we perform supervised fine-tuning on the Tulu-3 SFT OLMo-2 mixture (10% subsample, OLMo chat template, 1 epoch, learning rate 10^{-4} , AdamW). We again attach adapters to all module. For LoRA we sweep $r \in \{8, 16, 32, 64\}$ with $\alpha/r = 0.5$. For PLATE we sweep the following configuration $r \in \{32, 128, 512, 1024\}$, $\tau \in \{0.8, 0.9, 0.95, 0.98\}$.

We measure **OOD learnability** as IFEval accuracy and **OOD forgetting** as the drop in MATH-500 performance relative to the base model. In fact, although the Tulu-3 mixture dataset contains reasoning and maths problems, the MATH-500 benchmark was critically affected by forgetting. Again, highlighting the fact that given a dataset, predicting forgetting with respect to the OOD distribution is extremely hard.

Figure 5 shows that PLATE allows via increasing its number of learnable parameters to trade-off between learning and forgetting. It is also important to notice that for this experiment, the forgetting almost plateaus for PLATE while increasing the number of learnable parameters. In the low learnable parameters range, LoRA clearly outperforms PLATE in term of learnability. In contrast, LoRA is relatively insensitive to its rank in this setting: across the sweep, performance changes only modestly,

and forgetting remains hard to avoid. This helps explain why LoRA has become such a common default in recent years, its behavior is easy to predict and it tends to just work without careful hyperparameter tuning, albeit with an inherent retention cost. PLATE, on the other hand, is more delicate to configure precisely because it offers real control: its hyperparameters meaningfully move the model along the retention–plasticity spectrum, letting practitioners trade off new-task gains against preservation of prior behavior.

5.3 In-distribution forgetting benchmarks

We now consider settings where the task 1 distribution is known and forgetting can be measured directly on task 1 data after adapting to task 2.

5.3.1 Language modeling: WikiText-2 \rightarrow Middle English

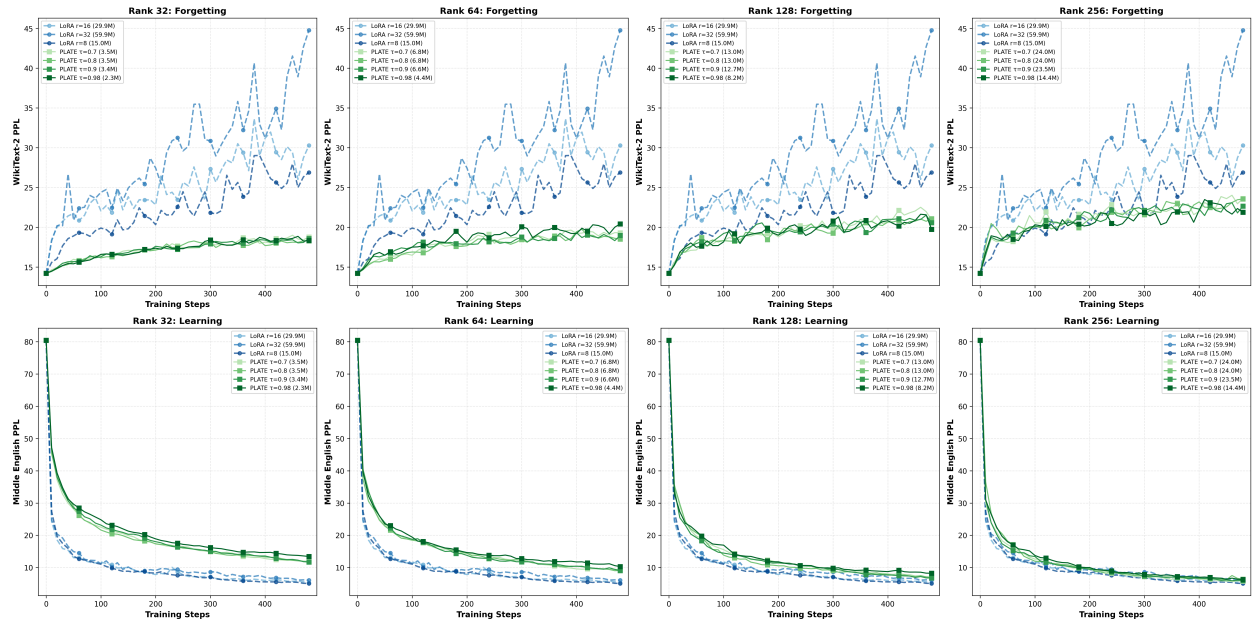


Figure 6: **Qwen 2.5-3B on Middle English (EN-ME):** Perplexity over training steps on WikiText-2 (top: retention/forgetting) and EN-ME (bottom: learning) Columns fix the PLATE output rank $r \in \{32, 64, 128, 256\}$ and sweep $\tau \in \{0.70, 0.80, 0.90, 0.98\}$ (green, solid) against LoRA baselines with varying ranks (blue, dashed). Top row reports WikiText-2 perplexity (forgetting) and bottom row reports Middle English perplexity (task learning), both over training steps.

We now study continual adaptation in a language generation task. We start from a pretrained Qwen 2.5-3B [29] model and fine-tune it on the Middle English dataset (EN-ME) for one epoch, comparing LoRA (varying rank) and PLATE (varying rank and τ). We measure **learnability** as perplexity on EN-ME, and **retention** as perplexity on WikiText-2 as a proxy for general-domain

pretraining behavior.² Figure 6 summarizes the resulting learning–retention trade-off. Across the sweep, LoRA achieves strong EN-ME learning but incurs substantially larger retention loss: WikiText-2 perplexity increases steadily with training, and the degradation typically worsens as rank grows. PLATE exhibits a clearer controllable spectrum. For a fixed rank r , increasing τ (stricter input constraint) consistently reduces WikiText-2 drift while preserving most of the EN-ME gains, whereas increasing r improves task learning but tends to raise forgetting. Overall, the results support our intended knob interpretation: r acts as the primary plasticity/forgetting control, and τ provides a secondary lever that can recover retention at a given r with comparatively smaller impact on learnability.

We now turn to controlled settings where the task 1 distribution is known and forgetting can be measured exactly. For these experiments, we train a randomly initialized model on task 1, and then fine-tune it on task 2 (Table 1).

5.3.2 Synthetic regression with tunable task dissimilarity

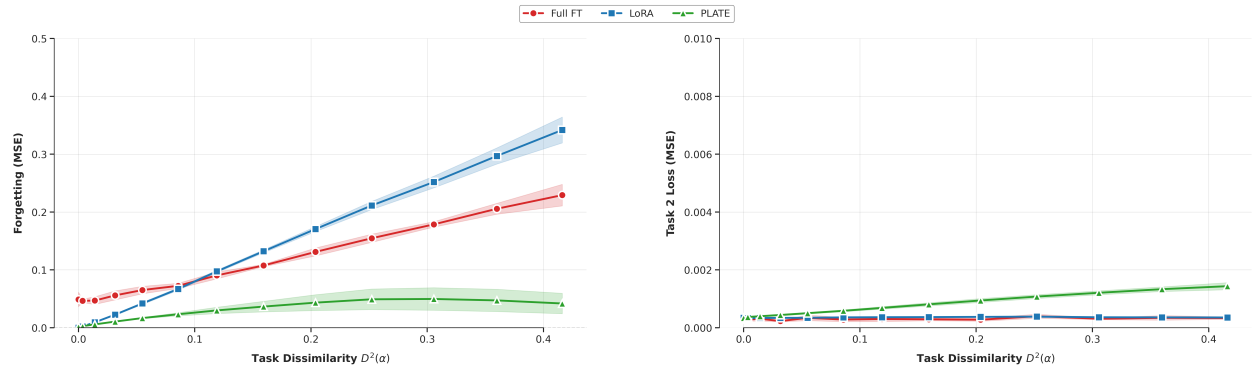


Figure 7: **Synthetic regression with tunable task dissimilarity:** (Left) forgetting on Task 1 (increase in MSE) versus task dissimilarity $D^2(\alpha)$; (Right) Task 2 test loss versus $D^2(\alpha)$. Forgetting for full FT (red) and LoRA (blue) grows roughly linearly with $D^2(\alpha)$, while PLATE (green) remains an order of magnitude smaller even for dissimilar tasks, with only a modest increase in Task 2 loss.

To explicitly vary task relatedness and capture how full fine-tuning, LoRA, and PLATE forget/learn when task 1 and task 2 dissimilarity increases. Concretely, we construct two regression tasks over Gaussian inputs $\mathbf{x} \sim \mathcal{N}(0, I_{100})$ with targets $f(\mathbf{x}) = \tanh(\mathbf{w}^\top \mathbf{x})$. Task 1 uses a fixed unit vector \mathbf{w}_1 while task 2 uses a rotated version of \mathbf{w}_1 where α relates to the rotation angle. Task dissimilarity is measured as $D^2(\alpha) = \mathbb{E}[(f_1(\mathbf{x}) - f_{2,\alpha}(\mathbf{x}))^2]$. We use a 2-layer tanh MLP (512 units). LoRA (rank 8) on all backbone layers, and PLATE ($r = 50$, $\tau = 0.6$); all methods train 100 epochs per task (Table 1).

Figure 7 shows forgetting and task 2 loss as a function of task dissimilarity, i.e., $D^2(\alpha)$. Full fine-tuning and LoRA exhibit approximately linear growth of forgetting with task dissimilarity; LoRA forgets even more than full fine-tuning despite using only a small subspace. PLATE, in contrast, keeps forgetting an order of magnitude smaller across the entire range, even when the

²While P_0 is not explicitly available for LLMs, WikiText-2 serves here as a proxy benchmark for broad English modeling ability.

tasks are nearly orthogonal, while having a slightly higher task 2 loss than the other methods. This synthetic experiment directly supports our theoretical picture: forgetting is governed by the geometry of the allowed update family S . In particular, restricting updates to be approximately data-orthogonal and concentrating plasticity on redundant degrees of freedom yields forgetting that grows only weakly with task drift.

5.3.3 Vision: MNIST 0-4 → 5-9

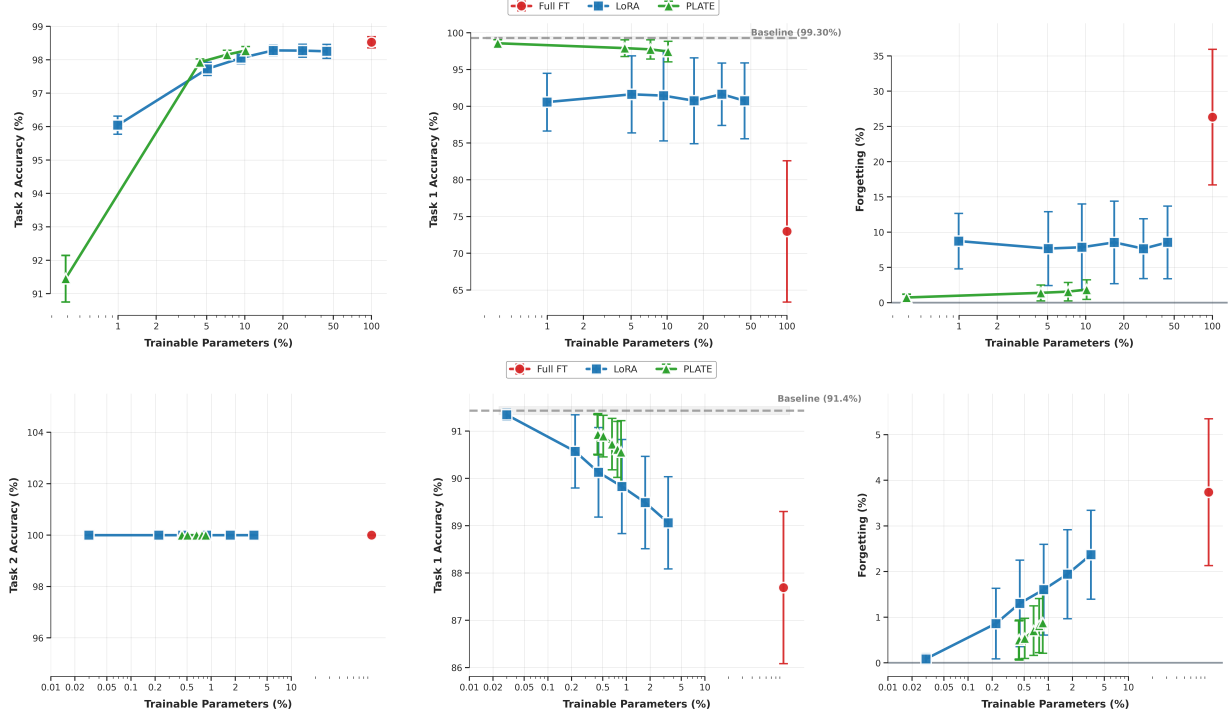


Figure 8: **In distribution Vision and text benchmarks:** (Top): MNIST 0-4→5-9, showing task 2 performance and task 1 forgetting as a function of trainable parameters. (Bottom): AG News→IMDB, with all methods achieving near-perfect task 2 accuracy while differing in how much they forget task 1.

For this experiment, task 1 is a classification problem on MNIST digits $\{0, \dots, 4\}$, and task 2 is the classification on MNIST digits $\{5, \dots, 9\}$ using a shared 3-layer ReLU MLP backbone (Table 1). We sweep LoRA ranks $r \in \{1, 8, 16, 32, 64, 128\}$ and PLATE ranks $r \in \{32, 64, 128, 256, 350\}$ (with $\tau = 0.8$), all applied to the backbone layers. Figure 8 (top) summarizes the results with respect to the % of learnable parameters. All methods reach $\approx 98\%$ task 2 accuracy once they have at least a few percent of the backbone parameters as trainable. The key difference lies in task 1 retention: full fine-tuning forgets about 26% of task 1 accuracy despite excellent task 2 performance; LoRA reduces forgetting to $\approx 7\text{-}9\%$. PLATE, by contrast, achieves near-full retention: at 10.2% trainable parameters it reaches 98.28% task 2 accuracy and 97.45% task 1 retention, i.e. only 1.85% forgetting, more than 4× better than LoRA at similar capacity.

5.3.4 Text classification: AG News \rightarrow IMDB

Finally we revisit the text modality in the *in-distribution* sense: we know both training and evaluation distributions for AG News (task 1) and IMDB (task 2) and can measure forgetting exactly. We pretrain DistilBERT-base [33] on AG News (3 epochs, learning rate 2×10^{-5}) obtaining a baseline task 1 accuracy of $91.34\% \pm 0.12\%$, then adapt to IMDB with: full fine-tuning; LoRA with $r \in \{1, 8, 16, 32, 64, 128\}$; and PLATE with fixed rank $r = 32$, thresholds $\tau \in \{0.6, 0.7, 0.8, 0.9\}$.

Figure 8 (bottom) shows that all methods reach 100% IMDB accuracy, so the trade-off is purely about task 1 retention. Full fine-tuning incurs about 3% forgetting. LoRA displays a rank-dependent trade-off: a rank-1 configuration achieves zero forgetting, but forgetting rises steadily to $\approx 2\text{-}3\%$ as rank increases. PLATE, by contrast, keeps forgetting below 0.5% across all configurations.

5.4 Computational Complexity Analysis

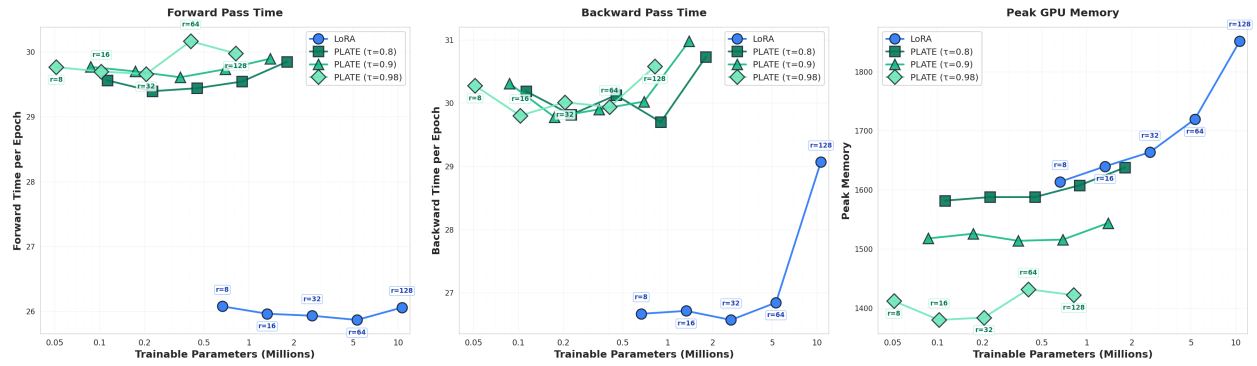


Figure 9: **Training efficiency of PLATE vs. LoRA on DistilBERT:** We adapt all linear layers and measure forward/backward time per epoch and peak GPU memory as a function of the total number of *trainable* adapter parameters (log scale). (i) For a fixed output rank r , PLATE trains only $A \in \mathbb{R}^{r \times k}$ and therefore uses rk trainable parameters per layer, whereas LoRA trains two matrices and uses $r(d_{\text{in}} + d_{\text{out}})$; across the sweep this yields fewer trainable parameters for PLATE, reducing optimizer-state and checkpoint size. (ii) Despite storing frozen bases Q , PLATE achieves lower peak GPU memory than LoRA in this setting, due to reduced optimizer states and a smaller adapter-induced activation footprint (only A is trainable). (iii) PLATE incurs a $\sim 10\text{--}15\%$ per-epoch time overhead, driven primarily by the extra projection through Q . (iv) Lowering τ (darker green) increases the induced basis dimension k and therefore increases memory, while leaving training time nearly unchanged. Overall, PLATE trades a modest compute overhead for substantially fewer trainable parameters, improved memory efficiency, and a trade-off between plasticity and memory retention.

We compare the additional compute and memory introduced by the adapter branch of LoRA and PLATE for a linear layer $W \in \mathbb{R}^{d_{\text{out}} \times d_{\text{in}}}$ and batch size n .

LoRA parameterizes a rank- r update as $\Delta W = B_\ell A_\ell$ with trainable $A_\ell \in \mathbb{R}^{r \times d_{\text{in}}}$ and $B_\ell \in \mathbb{R}^{d_{\text{out}} \times r}$, so each adapted layer introduces $r(d_{\text{in}} + d_{\text{out}})$ trainable parameters. In PLATE, the update is $\Delta W = BAQ^\top$ with a frozen input basis $Q \in \mathbb{R}^{d_{\text{in}} \times k}$, a trainable core $A \in \mathbb{R}^{r \times k}$, and a frozen output selector $B \in \mathbb{R}^{d_{\text{out}} \times r}$ (stored as a dense matrix in our implementation). This yields rk

trainable parameters per layer. For same r , when $k \ll d_{\text{in}} + d_{\text{out}}$, PLATE therefore reduces the number of trainable parameters and corresponding optimizer states by a large factor.

In the forward pass, LoRA applies ΔWx as $(xA^\top)B^\top$, which costs $\mathcal{O}(nd_{\text{in}}r + nrd_{\text{out}})$. In our PLATE implementation, the adapter branch is evaluated as

$$Z := xQ \in \mathbb{R}^{n \times k}, \quad U := ZA^\top \in \mathbb{R}^{n \times r}, \quad \Delta y := UB^\top \in \mathbb{R}^{n \times d_{\text{out}}},$$

implemented via dense `torch.nn.functional.linear` calls for both Q and B . Consequently, the adapter-branch forward cost is

$$\mathcal{O}(nd_{\text{in}}k + nkr + nrd_{\text{out}}).$$

This aligns with our empirical observation (see Figure 9) that PLATE incurs a modest training-time overhead driven primarily by the additional projection through Q .

Memory usage has three main components: optimizer states for trainable parameters, frozen adapter buffers, and saved activations needed for backpropagation. LoRA introduces two trainable matrices per adapted layer and therefore requires optimizer states for $r(d_{\text{in}} + d_{\text{out}})$ parameters, whereas PLATE trains only $A \in \mathbb{R}^{r \times k}$ and thus requires optimizer states for only rk parameters. PLATE additionally stores frozen buffers $Q \in \mathbb{R}^{d_{\text{in}} \times k}$ and $B \in \mathbb{R}^{d_{\text{out}} \times r}$ (stored densely in our implementation), which contribute $d_{\text{in}}k + d_{\text{out}}r$ in memory but do not create optimizer states.

Crucially, peak training memory is also driven by the activations that autograd must retain to form weight gradients. As a result, LoRA’s trainable down-projection requires retaining the full input activation $x \in \mathbb{R}^{n \times d_{\text{in}}}$ (in addition to smaller rank- r intermediates), and this cost accumulates across all adapted layers. In contrast, PLATE keeps both Q and B frozen and trains only A , so the adapter branch only needs to retain the projected activation $Z = xQ \in \mathbb{R}^{n \times k}$ to compute ∇A . When $k \ll d_{\text{in}}$, this reduces the adapter-induced activation footprint, and in our DistilBERT experiment the optimizer-state and activation savings dominate the additional frozen-basis storage, yielding lower peak GPU memory for PLATE across hyperparameters (see Figure 9). We also provide in Figure 10 PLATE initialization computational details.

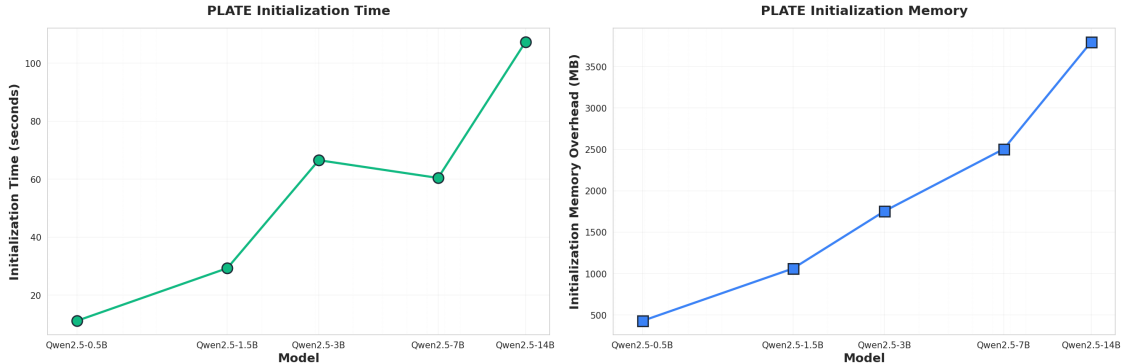


Figure 10: **Initialization complexity of PLATE adapters as a function of model size:** (left) Time (seconds) for computing Q matrices (via SRHT-based eigenproblem solving) and B selection matrices. (Right) Peak memory overhead during initialization, which includes both permanent adapter parameters and temporary computation buffers. Experiments conducted on Qwen2.5 models with fixed PLATE hyperparameters ($r = 64, \tau = 0.9$).

6 Discussion

The learning-forgetting trade-off can vary drastically across settings, depending on (*i*) the base model, (*ii*) the (often unknown) pretraining distribution, and (*iii*) the new-task distribution. As a result, it is difficult to anticipate performances a priori or to know in advance what fraction of parameters can be made trainable without incurring unacceptable forgetting. This sensitivity is especially pronounced in the LLMs regime, where P_0 is inaccessible and evaluation necessarily relies on proxies that only partially reflect pretraining-era capabilities.

In this context, LoRA remains appealing because it is simple, robust, and has been widely validated as a strong default for parameter-efficient adaptation. However, when retention is a first-class constraint, there is a clear need for methods that provide finer control over forgetting, even at the cost of more involved hyperparameter choices. PLATE is designed precisely for this setting: it exposes explicit knobs to navigate the retention-plasticity spectrum, rather than relying on a single rank parameter.

Empirically we observed that increasing the number of learnable output neurons r has a stronger impact on forgetting than changing the input energy threshold τ . Intuitively, enlarging r expands where the layer can change by making more neurons directly plastic, which more readily induces drift on pretraining-era behavior. By contrast, lowering τ relaxes the input-side constraint (increasing k and the number of trainable parameters) but, in practice, this added capacity tends to increase forgetting only mildly. In practice, r acts as the primary plasticity/forgetting knob, while τ is a secondary knob that mostly adjusts expressivity at comparatively smaller retention cost.

7 Conclusion

We studied catastrophic forgetting in parameter-efficient adaptation of foundation models in the practically relevant regime where the pretraining distribution P_0 is unavailable and replay is impractical. Our analysis isolates *functional drift on old inputs* as the central geometric driver of worst-case forgetting: as soon as an update family permits nonzero drift on P_0 , it necessarily contains directions that incur a nontrivial forgetting floor, while controlling drift also controls restricted curvature and yields an upper bound on worst-case forgetting. Together, these results suggest a simple principle for data-free continual learning: design update families that keep output drift on P_0 small.

Guided by this principle, we proposed PLATE, a structured PEFT adapter $\Delta W = BAQ^\top$ that is fully data-free with respect to P_0 : B concentrates plasticity on redundant output channels and Q restricts updates to a weight-derived low-energy input subspace computed once from frozen weights. Across controlled continual-learning benchmarks and LLM specialization, PLATE matches LoRA on new-task gains while substantially improving retention, and it exposes practical knobs to navigate the retention-plasticity spectrum. In practice, r (the number of plastic output channels) is the primary control for adaptation capacity and forgetting, while τ provides a secondary control that increases expressivity with a smaller retention cost.

Acknowledgements

We thank Sarath Shekkizhar, Adam Earle, Caiming Xiong, Shaul Druckmann, and Itamar Arel for insightful discussions and valuable feedback on this work.

References

- [1] Rahaf Aljundi, Francesca Babiloni, Mohamed Elhoseiny, Marcus Rohrbach, and Tinne Tuytelaars. Memory aware synapses: Learning what (not) to forget. In *Proceedings of the European conference on computer vision (ECCV)*, pages 139–154, 2018.
- [2] Randall Balestriero, Romain Cosentino, Behnaam Aazhang, and Richard Baraniuk. The geometry of deep networks: Power diagram subdivision. *Advances in Neural Information Processing Systems*, 32, 2019.
- [3] Arslan Chaudhry, Marc’Aurelio Ranzato, Marcus Rohrbach, and Mohamed Elhoseiny. Efficient lifelong learning with a-gem. *arXiv preprint arXiv:1812.00420*, 2018.
- [4] Mehrdad Farajtabar, Navid Azizan, Alex Mott, and Ang Li. Orthogonal gradient descent for continual learning. In *International conference on artificial intelligence and statistics*, pages 3762–3773. PMLR, 2020.
- [5] Jonathan Frankle and Michael Carbin. The lottery ticket hypothesis: Finding sparse, trainable neural networks. *arXiv preprint arXiv:1803.03635*, 2018.
- [6] Robert M French. Catastrophic forgetting in connectionist networks. *Trends in cognitive sciences*, 3(4):128–135, 1999.
- [7] Connall Garrod and Jonathan P Keating. The persistence of neural collapse despite low-rank bias. In *The Thirty-ninth Annual Conference on Neural Information Processing Systems*.
- [8] Ian J Goodfellow, Mehdi Mirza, Da Xiao, Aaron Courville, and Yoshua Bengio. An empirical investigation of catastrophic forgetting in gradient-based neural networks. *arXiv preprint arXiv:1312.6211*, 2013.
- [9] Yuling Gu, Oyvind Tafjord, Bailey Kuehl, Dany Haddad, Jesse Dodge, and Hannaneh Hajishirzi. Olmes: A standard for language model evaluations, 2025. URL <https://arxiv.org/abs/2406.08446>.
- [10] Song Han, Huizi Mao, and William J Dally. Deep compression: Compressing deep neural networks with pruning, trained quantization and huffman coding. *arXiv preprint arXiv:1510.00149*, 2015.
- [11] Song Han, Jeff Pool, John Tran, and William Dally. Learning both weights and connections for efficient neural network. *Advances in neural information processing systems*, 28, 2015.
- [12] Junxian He, Chunting Zhou, Xuezhe Ma, Taylor Berg-Kirkpatrick, and Graham Neubig. Towards a unified view of parameter-efficient transfer learning. *arXiv preprint arXiv:2110.04366*, 2021.
- [13] Torsten Hoefler, Dan Alistarh, Tal Ben-Nun, Nikoli Dryden, and Alexandra Peste. Sparsity in deep learning: Pruning and growth for efficient inference and training in neural networks. *Journal of Machine Learning Research*, 22(241):1–124, 2021.

[14] Neil Houlsby, Andrei Giurgiu, Stanislaw Jastrzebski, Bruna Morrone, Quentin De Laroussilhe, Andrea Gesmundo, Mona Attariyan, and Sylvain Gelly. Parameter-efficient transfer learning for nlp. In *International conference on machine learning*, pages 2790–2799. PMLR, 2019.

[15] Edward J Hu, Yelong Shen, Phillip Wallis, Zeyuan Allen-Zhu, Yuanzhi Li, Shean Wang, Lu Wang, Weizhu Chen, et al. Lora: Low-rank adaptation of large language models. *ICLR*, 1(2):3, 2022.

[16] Damjan Kalajdzievski. Scaling laws for forgetting when fine-tuning large language models. *arXiv preprint arXiv:2401.05605*, 2024.

[17] James Kirkpatrick, Razvan Pascanu, Neil Rabinowitz, Joel Veness, Guillaume Desjardins, Andrei A Rusu, Kieran Milan, John Quan, Tiago Ramalho, Agnieszka Grabska-Barwinska, et al. Overcoming catastrophic forgetting in neural networks. *Proceedings of the national academy of sciences*, 114(13):3521–3526, 2017.

[18] Brian Lester, Rami Al-Rfou, and Noah Constant. The power of scale for parameter-efficient prompt tuning. *arXiv preprint arXiv:2104.08691*, 2021.

[19] Hongbo Li, Sen Lin, Lingjie Duan, Yingbin Liang, and Ness B Shroff. Theory on mixture-of-experts in continual learning. *arXiv preprint arXiv:2406.16437*, 2024.

[20] Xiang Lisa Li and Percy Liang. Prefix-tuning: Optimizing continuous prompts for generation. *arXiv preprint arXiv:2101.00190*, 2021.

[21] David Lopez-Paz and Marc'Aurelio Ranzato. Gradient episodic memory for continual learning. *Advances in neural information processing systems*, 30, 2017.

[22] Michael McCloskey and Neal J Cohen. Catastrophic interference in connectionist networks: The sequential learning problem. In *Psychology of learning and motivation*, volume 24, pages 109–165. Elsevier, 1989.

[23] Seyed Iman Mirzadeh, Mehrdad Farajtabar, Razvan Pascanu, and Hassan Ghasemzadeh. Understanding the role of training regimes in continual learning. *Advances in Neural Information Processing Systems*, 33:7308–7320, 2020.

[24] Ari Morcos, Maithra Raghu, and Samy Bengio. Insights on representational similarity in neural networks with canonical correlation. *Advances in neural information processing systems*, 31, 2018.

[25] Team Olmo, Allyson Ettinger, Amanda Bertsch, Bailey Kuehl, David Graham, David Heineman, Dirk Groeneveld, Faeze Brahman, Finbarr Timbers, Hamish Ivison, et al. Olmo 3. *arXiv preprint arXiv:2512.13961*, 2025.

[26] Team OLMO, Pete Walsh, Luca Soldaini, Dirk Groeneveld, Kyle Lo, Shane Arora, Akshita Bhagia, Yuling Gu, Shengyi Huang, Matt Jordan, Nathan Lambert, Dustin Schwenk, Oyvind Tafjord, Taira Anderson, David Atkinson, Faeze Brahman, Christopher Clark, Pradeep Dasigi, Nouha Dziri, Allyson Ettinger, Michal Guerquin, David Heineman, Hamish Ivison, Pang Wei Koh, Jiacheng Liu, Saumya Malik, William Merrill, Lester James V. Miranda, Jacob Morrison, Tyler Murray, Crystal Nam, Jake Poznanski, Valentina Pyatkin, Aman Rangapur, Michael

Schmitz, Sam Skjonsberg, David Wadden, Christopher Wilhelm, Michael Wilson, Luke Zettlemoyer, Ali Farhadi, Noah A. Smith, and Hannaneh Hajishirzi. 2 olmo 2 furious, 2025. URL <https://arxiv.org/abs/2501.00656>.

[27] German I Parisi, Ronald Kemker, Jose L Part, Christopher Kanan, and Stefan Wermter. Continual lifelong learning with neural networks: A review. *Neural networks*, 113:54–71, 2019.

[28] Fuli Qiao and Mehrdad Mahdavi. Learn more, but bother less: parameter efficient continual learning. *Advances in Neural Information Processing Systems*, 37:97476–97498, 2024.

[29] Qwen, :, An Yang, Baosong Yang, Beichen Zhang, Binyuan Hui, Bo Zheng, Bowen Yu, Chengyuan Li, Dayiheng Liu, Fei Huang, Haoran Wei, Huan Lin, Jian Yang, Jianhong Tu, Jianwei Zhang, Jianxin Yang, Jiaxi Yang, Jingren Zhou, Junyang Lin, Kai Dang, Keming Lu, Keqin Bao, Kexin Yang, Le Yu, Mei Li, Mingfeng Xue, Pei Zhang, Qin Zhu, Rui Men, Runji Lin, Tianhao Li, Tianyi Tang, Tingyu Xia, Xingzhang Ren, Xuancheng Ren, Yang Fan, Yang Su, Yichang Zhang, Yu Wan, Yuqiong Liu, Zeyu Cui, Zhenru Zhang, and Zihan Qiu. Qwen2.5 technical report, 2025. URL <https://arxiv.org/abs/2412.15115>.

[30] Roger Ratcliff. Connectionist models of recognition memory: constraints imposed by learning and forgetting functions. *Psychological review*, 97(2):285, 1990.

[31] Andrei A Rusu, Neil C Rabinowitz, Guillaume Desjardins, Hubert Soyer, James Kirkpatrick, Koray Kavukcuoglu, Razvan Pascanu, and Raia Hadsell. Progressive neural networks. *arXiv preprint arXiv:1606.04671*, 2016.

[32] Gobinda Saha, Isha Garg, and Kaushik Roy. Gradient projection memory for continual learning. *arXiv preprint arXiv:2103.09762*, 2021.

[33] Victor Sanh, Lysandre Debut, Julien Chaumond, and Thomas Wolf. Distilbert, a distilled version of bert: smaller, faster, cheaper and lighter, 2020. URL <https://arxiv.org/abs/1910.01108>.

[34] Nitish Srivastava, Geoffrey Hinton, Alex Krizhevsky, Ilya Sutskever, and Ruslan Salakhutdinov. Dropout: a simple way to prevent neural networks from overfitting. *The journal of machine learning research*, 15(1):1929–1958, 2014.

[35] Xiao Wang, Tianze Chen, Qiming Ge, Han Xia, Rong Bao, Rui Zheng, Qi Zhang, Tao Gui, and Xuan-Jing Huang. Orthogonal subspace learning for language model continual learning. In *Findings of the Association for Computational Linguistics: EMNLP 2023*, pages 10658–10671, 2023.

[36] Yibo Yang, Xiaojie Li, Zhongzhu Zhou, Shuaiwen Song, Jianlong Wu, Liqiang Nie, and Bernard Ghanem. Corda: Context-oriented decomposition adaptation of large language models for task-aware parameter-efficient fine-tuning. *Advances in Neural Information Processing Systems*, 37:71768–71791, 2024.

[37] Jaehong Yoon, Eunho Yang, Jeongtae Lee, and Sung Ju Hwang. Lifelong learning with dynamically expandable networks. *arXiv preprint arXiv:1708.01547*, 2017.

[38] Haoran You, Randall Balestriero, Zhihan Lu, Yutong Kou, Huihong Shi, Shunyao Zhang, Shang Wu, Yingyan Celine Lin, and Richard Baraniuk. Max-affine spline insights into deep network pruning. *arXiv preprint arXiv:2101.02338*, 2021.

- [39] Guanxiong Zeng, Yang Chen, Bo Cui, and Shan Yu. Continual learning of context-dependent processing in neural networks. *Nature Machine Intelligence*, 1(8):364–372, 2019.
- [40] Friedemann Zenke, Ben Poole, and Surya Ganguli. Continual learning through synaptic intelligence. In *International conference on machine learning*, pages 3987–3995. PMLR, 2017.
- [41] Linglan Zhao, Xuerui Zhang, Ke Yan, Shouhong Ding, and Weiran Huang. Safe: Slow and fast parameter-efficient tuning for continual learning with pre-trained models. *Advances in Neural Information Processing Systems*, 37:113772–113796, 2024.

A Proofs

A.1 Proof of Proposition 1

Proof. Recall that for each layer ℓ we have

$$z_\theta^{(\ell)}(x) = W^{(\ell)} h_\theta^{(\ell-1)}(x), \quad h_\theta^{(\ell)}(x) = \sigma(z_\theta^{(\ell)}(x)),$$

and that $\theta_1 = \theta_0 + \Delta\theta$ with $\Delta\theta = \{\Delta W^{(\ell)}\}_\ell$.

We prove by induction on ℓ that for every $x \in \text{supp}(P_0)$,

$$h_{\theta_1}^{(\ell)}(x) = h_{\theta_0}^{(\ell)}(x).$$

Base case ($\ell = 1$). By definition,

$$z_{\theta_1}^{(1)}(x) = (W^{(1)} + \Delta W^{(1)}) h_{\theta_1}^{(0)}(x) = (W^{(1)} + \Delta W^{(1)}) x.$$

Using the per-neuron orthogonality condition (1) with $h_{\theta_0}^{(0)}(x) = x$ gives $\Delta W^{(1)}x = 0$, hence

$$z_{\theta_1}^{(1)}(x) = W^{(1)}x = z_{\theta_0}^{(1)}(x),$$

and therefore $h_{\theta_1}^{(1)}(x) = h_{\theta_0}^{(1)}(x)$.

Induction step. Assume that for some $\ell \geq 1$ we have $h_{\theta_1}^{(\ell-1)}(x) = h_{\theta_0}^{(\ell-1)}(x)$ for all $x \in \text{supp}(P_0)$. Then

$$\begin{aligned} z_{\theta_1}^{(\ell)}(x) &= (W^{(\ell)} + \Delta W^{(\ell)}) h_{\theta_1}^{(\ell-1)}(x) \\ &= (W^{(\ell)} + \Delta W^{(\ell)}) h_{\theta_0}^{(\ell-1)}(x) \\ &= W^{(\ell)} h_{\theta_0}^{(\ell-1)}(x) + \Delta W^{(\ell)} h_{\theta_0}^{(\ell-1)}(x). \end{aligned}$$

By the per-neuron orthogonality condition (1), $\Delta W^{(\ell)} h_{\theta_0}^{(\ell-1)}(x) = 0$ for all $(x, y) \sim P_0$, so

$$z_{\theta_1}^{(\ell)}(x) = W^{(\ell)} h_{\theta_0}^{(\ell-1)}(x) = z_{\theta_0}^{(\ell)}(x).$$

Thus $h_{\theta_1}^{(\ell)}(x) = h_{\theta_0}^{(\ell)}(x)$.

In particular, the final layer outputs coincide for all $x \in \text{supp}(P_0)$:

$$f_{\theta_1}(x) = f_{\theta_0}(x),$$

which implies $L_0(\theta_1) = L_0(\theta_0)$ and therefore $\mathcal{F}_0(\theta_0, \theta_1) = 0$. \square

A.2 Curvature assumption and proof of Theorem 1

Assumption 1 (Output-space curvature link). There exists a constant $\mu_0 > 0$ such that for all $\Delta\theta \in S$

$$\Delta\theta^\top H_0 \Delta\theta \geq \mu_0 \mathbb{E}_{x \sim P_0} [\|J_{\theta_0}(x)\Delta\theta\|_2^2]. \quad (4)$$

Intuitively, directions in parameter space that induce a large first-order change in the network output on P_0 must incur a proportional amount of curvature in the old-task loss L_0 .

Recall the definition of $\varepsilon(S)$ from (2),

$$\varepsilon(S) := \sup_{\substack{\Delta\theta \in S \\ \|\Delta\theta\|_2=1}} \left(\mathbb{E}_{x \sim P_0} [\|J_{\theta_0}(x)\Delta\theta\|_2^2] \right)^{1/2}. \quad (5)$$

Proof. Define

$$\Phi(\Delta\theta) := \left(\mathbb{E}_{x \sim P_0} [\|J_{\theta_0}(x)\Delta\theta\|_2^2] \right)^{1/2}.$$

Φ is continuous and the feasible set $\{\Delta\theta \in S : \|\Delta\theta\|_2 = 1\}$ is compact, so the supremum in Eq.2 is attained. Thus there exists $\Delta\theta^* \in S$ with $\|\Delta\theta^*\|_2 = 1$ such that

$$\Phi(\Delta\theta^*) = \varepsilon(S). \quad (6)$$

For a given step size $\rho > 0$, consider the scaled update $\Delta\theta_\rho := \rho\Delta\theta^* \in S$ so that $\|\Delta\theta_\rho\|_2 = \rho$. We have,

$$\mathbb{E}_{x \sim P_0} [\|J_{\theta_0}(x)\Delta\theta_\rho\|_2^2] = \rho^2 \mathbb{E}_{x \sim P_0} [\|J_{\theta_0}(x)\Delta\theta^*\|_2^2] = \rho^2 \varepsilon(S)^2.$$

Applying Assumption 1 to $\Delta\theta_\rho$ yields

$$\Delta\theta_\rho^\top H_0 \Delta\theta_\rho \geq \mu_0 \mathbb{E}_{x \sim P_0} [\|J_{\theta_0}(x)\Delta\theta_\rho\|_2^2] = \mu_0 \rho^2 \varepsilon(S)^2. \quad (7)$$

Using the Taylor expansion with $\Delta\theta = \Delta\theta_\rho$ and $g_0 \approx 0$ gives

$$\begin{aligned} \mathcal{F}_0(\theta_0, \theta_0 + \Delta\theta_\rho) &= L_0(\theta_0 + \Delta\theta_\rho) - L_0(\theta_0) \\ &= g_0^\top \Delta\theta_\rho + \frac{1}{2} \Delta\theta_\rho^\top H_0 \Delta\theta_\rho + R(\Delta\theta_\rho). \end{aligned} \quad (8)$$

For a well-trained model we take $g_0 \approx 0$ and neglect the linear term. We obtain

$$\begin{aligned} \mathcal{F}_0(\theta_0, \theta_0 + \Delta\theta_\rho) &\geq \frac{1}{2} \mu_0 \rho^2 \varepsilon(S)^2 - C_T \rho^3 \\ &= \left(\frac{\mu_0}{2} \right) \rho^2 \varepsilon(S)^2 - C_T \rho^3. \end{aligned}$$

□

A.3 Proof of Proposition 2

Proof. This follows directly from the explicit Deep Neural Collapse solution form derived in [7], where each row direction is expressed (up to scale) as a linear combination of the layerwise prototype directions; see the displayed derivation yielding $w_j^{(\ell)} \propto \sum_{c=1}^K O_{cj} \mu_c^{(\ell)}$. □

A.4 Proof of Proposition 3

Proof. For any $\Delta\theta \in S$ with $\|\Delta\theta\| \leq \rho$, since we have $g_0 = \nabla_\theta L_0(\theta_0) \approx 0$

$$\mathcal{F}_0(\theta_0, \theta_0 + \Delta\theta) = \frac{1}{2} \Delta\theta^\top H_0 \Delta\theta + O(\Delta\theta^3)$$

By definition of $\lambda(S)$, $\Delta\theta^\top H_0 \Delta\theta \leq \lambda(S) \|\Delta\theta\|^2 \leq \lambda(S) \rho^2$. Thus

$$\mathcal{F}_0(\theta_0, \theta_0 + \Delta\theta) \leq \frac{\lambda(S)}{2} \rho^2 + O(\rho^3).$$

The unconstrained case follows from $\lambda(\mathbb{R}^{\dim(\theta)}) = \lambda_{\max}$. □

A.5 Proof of Proposition 4

Proof. Recall that

$$L_0(\theta) = \mathbb{E}_{(x,y) \sim P_0} [\ell(f_\theta(x), y)], \quad H_0 = \nabla_\theta^2 L_0(\theta_0) = \mathbb{E}_{(x,y) \sim P_0} [\nabla_\theta^2 \ell(f_\theta(x), y)]_{\theta=\theta_0}.$$

Fix (x, y) and define $\phi(\theta) := \ell(f_\theta(x), y)$. Then

$$\nabla_\theta^2 \phi(\theta) = J_\theta(x)^\top \nabla_f^2 \ell(f_\theta(x), y) J_\theta(x) + \sum_{i=1}^{d_{\text{out}}} \frac{\partial \ell}{\partial f_i}(f_\theta(x), y) \nabla_\theta^2 f_{\theta,i}(x), \quad (9)$$

where $J_\theta(x) = \nabla_\theta f_\theta(x)$ and $f_{\theta,i}(x)$ denotes the i -th output coordinate.

The second term in (9) is the only deviation from Gauss–Newton curvature, and it is weighted by the loss sensitivity to the model output. For a well-optimized pretrained model on the old distribution, this output sensitivity is small on old-task data, so we treat the second term as a residual curvature contribution. Concretely, we assume that along the update directions of interest this residual contribution is uniformly bounded by a constant R (and in the idealized case of zero loss on P_0 , it vanishes). Therefore, evaluating (9) at $\theta = \theta_0$ the per-sample Hessian is upper bounded by the first term plus an additive residual of size at most R which we will assume to be 0 for clarity.

Now, using $\nabla_f^2 \ell(f_{\theta_0}(x), y) \preceq \beta I$ we have for any vector v

$$v^\top \nabla_\theta^2 \ell(f_{\theta_0}(x), y) v = (J_{\theta_0}(x)v)^\top \nabla_f^2 \ell(f_{\theta_0}(x), y) (J_{\theta_0}(x)v) \leq \beta \|J_{\theta_0}(x)v\|_2^2.$$

Taking expectation over $(x, y) \sim P_0$ gives

$$v^\top H_0 v = \mathbb{E}_{(x,y) \sim P_0} [v^\top \nabla_\theta^2 \ell(f_{\theta_0}(x), y) v] \leq \beta \mathbb{E}_{x \sim P_0} [\|J_{\theta_0}(x)v\|_2^2].$$

Now restrict to $v \in S$ with $\|v\|_2 = 1$ and take the supremum

$$\lambda(S) = \sup_{\substack{v \in S \\ \|v\|_2=1}} v^\top H_0 v \leq \beta \sup_{\substack{v \in S \\ \|v\|_2=1}} \mathbb{E}_{x \sim P_0} [\|J_{\theta_0}(x)v\|_2^2] = \beta \varepsilon(S)^2.$$

□

A.6 Proof of Theorem 2

Proof. By Proposition 3, there exist $\rho > 0$ such that for any linear subspace S

$$\mathcal{F}_{\max}(S, \rho) \leq \frac{\lambda(S)}{2} \rho^2 + C \rho^3.$$

Under $\nabla_f^2 \ell(f_{\theta_0}(x), y) \preceq \beta I$, Proposition 4 yields $\lambda(S) \leq \beta \varepsilon(S)^2$. Substituting this into the previous display gives

$$\mathcal{F}_{\max}(S, \rho) \leq \frac{\beta}{2} \varepsilon(S)^2 \rho^2 + O(\rho^3),$$

□

Table 1: Domain-specific experimental configurations. All experiments follow Algorithm 2 with $K = 10$ runs.

Domain	Tasks $\mathcal{D}_1 \rightarrow \mathcal{D}_2$	Architecture	Epochs (E_1/E_2)	Learning Rate	Batch Size
Vision	MNIST 0-4 \rightarrow 5-9 (5 classes each)	3-layer ReLU MLP (784 \rightarrow 256 \rightarrow 256 \rightarrow 256) + two 256 \rightarrow 5 heads	10/10	10^{-3} (Adam)	128
NLP (small)	AG News \rightarrow IMDB (4 classes \rightarrow 2 classes)	DistilBERT-base (6 layers, 768-dim) + two linear heads (768 \rightarrow 4/2)	3/3	2×10^{-5} (AdamW, 10% warmup)	32
Regression	$f_1(\mathbf{x}) \rightarrow f_2^*(\mathbf{x})$ on Gaussian inputs ($d = 100$)	2-layer tanh MLP (100 \rightarrow 512 \rightarrow 512) + two 512 \rightarrow 1 heads	100/100	10^{-3} (Adam)	128
LLM	WikiText-2 \rightarrow Middle English (EN-ME)	Qwen/Qwen2.5-3B (Causal LM), adapters on attention/MLP projections	0/1	10^{-3} (AdamW)	16

Table 2: Hyperparameter grids and target modules for each adaptation method.

Method	Hyperparameter	Values
LoRA	Rank r	Vision/Regression/NLP: {1, 8, 16, 32, 64, 128}; LLM: {8, 16, 32}
	Scaling α	$\alpha/r = 0.5$
	Target modules	Vision/Regression/NLP: all linear layers; LLM: attention and MLP projections (e.g., <code>q</code> , <code>k</code> , <code>v</code> , <code>o</code> , <code>up</code> , <code>down</code> , <code>gate</code>).
PLATE	Rank r	Vision: {32, 64, 128, 256, 350}; NLP: 32; Regression: 50; LLM: {32, 64, 128, 256}
	Energy threshold τ	Vision/NLP: {0.6, 0.7, 0.8, 0.9}; LLM: {0.70, 0.80, 0.90, 0.98}.
	Max rank r_{\max}	{256, 512}
	Scaling ρ	0.5
Full FT	Target modules	Vision/Regression/NLP: all linear layers.
	Trainable parameters	All parameters.

B Experimental Details

Algorithm 2 Parameter-efficient two-task continual learning protocol

Require: $\mathcal{D}_1, \mathcal{D}_2$, base model f_θ , heads h_1, h_2 , methods $\mathcal{M} = \{\text{Full-FT, LoRA, PLATE}\}$, configs \mathcal{C}_m

- 1: **for** $k = 1$ to K **do**
- 2: Initialize $f_\theta^{(k)}, h_1^{(k)}, h_2^{(k)}$
- 3: **Stage 1:** train $(f_\theta^{(k)}, h_1^{(k)})$ on \mathcal{D}_1 for E_1 epochs
- 4: Record baseline Task 1 accuracy and save checkpoint $\theta_1^{(k)}$
- 5: **for** method $m \in \mathcal{M}$ **do**
- 6: **for** config $c \in \mathcal{C}_m$ **do**
- 7: Restore $f_{\theta^{(k)}} \leftarrow f_{\theta_1^{(k)}}$, freeze $h_1^{(k)}$
- 8: Apply adapters for (m, c) to $f_{\theta^{(k)}}$ and define trainable set Θ (plus $h_2^{(k)}$)
- 9: **Stage 2:** train $(f_{\theta^{(k)}}, h_2^{(k)})$ on \mathcal{D}_2 for E_2 epochs
- 10: Evaluate Task 2 (learnability) & Task 1 (forgetting)
- 11: **end for**
- 12: **end for**
- 13: **end for**
- 14: Aggregate means and standard deviations across k for each (m, c)
